

REVIEWS OF TOPICAL PROBLEMS

PACS numbers: **02.70. – c,** 02.70.Uu, 13.85.Lg

Integral hadron–nuclear cross sections

A.V. Bagulya, V.M. Grichine, V.N. Ivanchenko

DOI: https://doi.org/10.3367/UFNe.2025.09.040030

Contents

Abstract. Hadron–nucleus cross sections determine the hadron shower development in matter. Here we describe cross section models developed in the framework of the Geant4 toolkit, that is the main software package used for simulation of the LHC experiments. The simulation accuracy contributes to the systematic uncertainty of the experimental measurements. Other applications including the NICA collider experiments are discussed in terms of the Geant4 parameterisation method accuracy for the hadron–nucleus cross sections. It is shown that the parameterisations used are applicable in a wide energy range from threshold to very high energies and for all materials utilized in the experimental facilities.

Keywords: Geant4, hadron, nucleon, nucleus, cross section

1. Introduction

Calculating hadron–nucleon and hadron–nuclear cross sections, particularly integral cross sections, is of great importance for applications in particle physics, nuclear physics, and nuclear medicine. The integral hadron–nucleon and hadron–nuclear cross sections determine the mean free path of a hadron in relation to the strong interaction with a nucleon and nucleus, respectively. In addition to their application in calculating the hadron calorimeter parameters, they are used to construct the final state in cascade and string models.

The integral hadron–nucleon/nuclear cross sections, being one of the main characteristics of the strong interaction, have been actively discussed in the literature (see reviews in *Phys. Usp* [1–3], *PEPAN* [4], and the references therein). A significant step towards the construction of practical models of the integral hadron–nucleon/nuclear cross sections was the article by B.Z. Kopeliovich [5], in which R. Glauber's [6] diffraction theory of multiple scattering of an incident hadron in a nucleus was related to V.N. Gribov's [7] correction for the inelastic screening effect. It turned out that the formalism developed in [5] can be simplified in such a way that the end result is a universal practical model describing an almost complete set of integral hadron–nucleus cross sections in wide ranges of the hadron energy and nuclear atomic weight (see Section 2.2.2).

From an experimental perspective, the integral hadron–nucleon and hadron–nucleus cross sections were discussed in periodic reviews of the Particle Data Group (PDG [8]) and the monographs by V.S. Barashenkov and V.D. Toneev [9], respectively.

The Geant4 software package [10–12] is designed for Monte Carlo simulations of the propagation of particles through materials organized into complex geometric structures. This package is widely used in high-energy physics, nuclear and accelerator physics, as well as in space and medical research. Initially, the main priority of Geant4 was to provide simulations for experiments at the LHC. The integral cross sections of hadron–nucleon/nuclear interactions significantly affect the precision of the description of hadron showers in calorimeters, as well as the hadron interactions in a thin target geometry.

Historically, the first model of integral nuclear cross sections [10] in Geant4 was a model based on parameterization developed in the GHEISHA software package [13] (the LHEP-model in Geant4). Subsequently, empirical parameterizations [14] (the AHPW-model) and more advanced parameterizations by Barashenkov [15, 16] were implemented for nucleons and pions. The later proposed approach of the final-state chiral phase space, the CHIPS-model [17], had the advantage of more accurate modeling of the integral and differential hadron–nucleon cross sections in the resonance region. Parameterizations in the CHIPS-model for hadron–nucleon interactions were adjusted to better match the simplified Glauber–Gribov model [18] (GG-model in Geant4) describing the integral hadron/nucleus–nucleus cross sections.

A.V. Bagulya [(1,2,*)], **V.M. Grichine** [(1)], **V.N. Ivanchenko** [(2)]
[(1)] Lebedev Physical Institute, Russian Academy of Sciences, Leninskii prosp. 53, 119991 Moscow, Russian Federation
[(2)] Tomsk State University, prosp. Lenina 36, 634050 Tomsk, Russian Federation
E-mail: [(*)] bagulyaav@lebedev.ru

Received 16 June 2025
Uspekhi Fizicheskikh Nauk **196** (2) 115 – 124 (2026)
Translated by V.N. Ivanchenko

At low energies, cross sections based on global databases are used. The HP (High Precision) sub-package is used to model the neutron propagation in matter. The partial cross sections for elastic, inelastic, absorption, and fission nuclei in the latest versions of Geant4 are based on the JEFF-3.3 [25] database. Unlike V.S. Barashenkov's parametrizations, prepared for elements and consisting of natural isotope compositions, in the HP data all cross sections are given for individual isotopes. Data are available for the energy range 10^{-6} eV–20 MeV. Molecular scattering cross sections [26] are used to simulate the elastic scattering of thermal neutrons. The HP sub-package was extended [12] by adding inelastic cross sections for protons and light ions for energies below 200 MeV using the TENDL–2023 database [28].

Since HP data operations are relatively slow, a method was developed to convert HP cross sections into a compact internal XS database [27], which contains cross sections for elements and isotopes. These cross sections are used by default in Geant4 for neutrons. The cross sections for the inelastic interactions of protons, deuterons, tritons, and helium nuclei can be used if required for a specific application.

Subsequently, a generalized method developed to describe cross sections for all hadrons and any energies in Geant4 [12], which is currently the main method. The hadron–nucleus cross sections are constructed based on the parameterizations of Barashenkov and the Glauber–Gribov model, newly developed in Geant4, which is based on the parameterization of hadron–nucleon cross sections measured with good accuracy for protons, pions, and kaons. These cross sections are used to parameterize the cross sections of other hadrons.

Originally developed for applications in high-energy physics, particularly for experiments at the LHC, the Geant4 package has found wide application in nuclear physics, medicine, and space exploration. Developers have increasingly faced the challenge of describing physical processes over a wide energy range, for hadron processes from a few MeV to hundreds of TeV, and in materials with atomic numbers in the range 1–100. This review discusses the current state of the integrated hadron–nucleon/nuclear cross section models, the result of more than 25 years of development of the Geant4 software package. The model calculations are compared with the experimental data.

2. Cross section models

2.1 Hadron–nucleon cross sections

2.1.1 Nucleon–nucleon and meson–nucleon cross sections. Direct approximations of the experimental data are used for nucleons, pions, and kaons. Parameterization is performed in terms of

$$x = \ln\left(\frac{P}{P_0}\right),$$

where P is momentum of the hadron, and $P_0 = 1$ GeV [17]. The dependencies of the integral total, inelastic, and elastic cross sections on the hadron momentum can be subdivided into three regions: low-energy, resonances, and high-energy. In the low-energy and the resonance regions, Breit–Wigner functions for resonances and polynomials for the background are used. The Breit–Wigner peaks are somewhat smoothed to better match the GG-model.

Experimental data show a relativistic increase of the hadron–nucleon cross sections at energies greater than ~ 100 GeV. This increase is associated with the discovery of new channels of inelastic interactions, in particular the formation of pairs of new heavy particles. However, this increase is limited by the unitary condition and ceases with further increases in energy for a given value of the transverse impact parameter. What remains is an increase in the interaction radius. A possible mechanism for this, derived from quantum chromo-dynamics, is the relativistic increase in the hadron radius due to parton diffusion in impact parameter space due to the emission of increasingly slower partons in the comb-type diagrams [3]. This mechanism leads to a logarithmic increase in the integral cross sections as a function of the total energy at the center of mass of the hadron and nucleon. Therefore, in the high-energy region above approximately 30 GeV, the parameterizations recommended by the PDG group [8] are used. The form of these parameterizations precisely corresponds to this mechanism. The specific numerical form of the parameterizations and the numerical values of the parameters can be found in the software implementations of the Geant4 package (see Section 2.3). These parameterizations are used in most of the 'physics lists' (sets of physical processes and particles) of the Geant4 package.

2.1.2 Cross sections for heavy baryons and mesons off nucleons. Based on the argument of simplified quark additivity [19, 20], one can assume that the relative contribution of light quarks, $\langle \tilde{u}, \tilde{d} \rangle$, to the total proton–proton cross section, σ_{tot}^{pp}, is approximately equal to $\sigma_u \sim \sigma_d = \sigma_{tot}^{pp}/3$, i.e., $\langle \tilde{u}, \tilde{d} \rangle = 1/3$. Then, for baryons with one s-quark (Λ, Σ):

$$\tilde{s} + \frac{1}{3} + \frac{1}{3} = 0.88\,, \quad \tilde{s} \simeq 0.21\,, \tag{1}$$

where $\tilde{s}$ is the relative contribution of the s-quark to the cross section, and the value 0.88 is the experimentally measured average ratio of the integral total $\Lambda - p$ and $p - p$ cross sections in the energy range of 10–1000 GeV. For baryons with two s-quarks (Ξ), we have:

$$2\tilde{s} + \frac{1}{3} = 0.76\,, \tag{2}$$

in satisfactory agreement with the experimental data [21] (Table 1). A weak dependence of the relative quark contribution to the integral cross section on the ratio of its mass to the mass of the light quark, $m_s/m_{\langle u,d\rangle} \simeq 25$, is evident, where m_s is the mass of the s quark and $m_{\langle u,d\rangle}$ is the average mass of the u- and d-quarks. Then, for simplicity, we can assume a linear dependence of the relative contribution on the logarithm of the quark mass ratio:

$$\langle \tilde{u}, \tilde{d} \rangle, \tilde{s}, \tilde{c}, \tilde{b} = \frac{1}{3} + a \ln \frac{m_{\langle u,d\rangle, s, c, b}}{m_{\langle u,d\rangle}}\,, \tag{3}$$

for s-quark correspondingly,

$$\tilde{s}\colon\ 0.21 = 0.33 + a \ln(25)\,. \tag{4}$$

The last equation defines the coefficient a. From the relation (3), one can derive the relative contributions of the c- and b-quarks, shown in Tables 1 and 2. Then, the integral cross sections of heavy baryons/mesons on nucleons can be derived from the known nucleon/meson–nucleon cross sections by introducing simple correction factors (or their combinations), given in Table 2. The relation (3) still awaits confirmation or refutation by experiment in processes involving the c- and b-quarks.

Table 1. Ratio of total cross sections $\Xi^- - p$ Geant4 corresponding to quark additivity to experimental data [21] ($\sigma_{tot}^{\Xi^- p}/\sigma_{tot}^{pp} = 0.76$).

Computational and experimental ratios $\sigma_{tot}^{\Xi^- p}/\sigma_{tot}^{pp}$		
Ξ^- momentum, GeV/c	$\sigma_{tot}^{\Xi^- p}/\sigma_{tot}^{pp}$ (Geant4)	$\sigma_{tot}^{\Xi^- p}/\sigma_{tot}^{pp}$ (experiment)
101.5	0.76	0.758
133.8	0.76	0.759

Table 2. Ratio of total hyperon–proton (Hp) to proton–proton cross sections corresponding to quark additivity versus the number of heavy quarks.

$\sigma_{tot}^{Hp}/\sigma_{tot}^{pp}$ versus heavy quark number			
Number/flavour	1	2	3
strangeness	0.88 (Λ)	0.76 (Ξ)	0.64 (Ω)
charm	0.784	0.569	0.353
beauty	0.74	0.481	0.222

2.2 Hadron–nucleus cross section in Geant4

2.2.1 Optical model. Barashenkov's interpolations [15, 16] (B-model) for the integral total and inelastic nucleon/pion–nucleus cross sections make substantial use of the quasi-optical model parameterization in the region of hadron kinetic energies ($T > 10$ MeV) and the phenomenological assumption that the cross section, $\sigma \sim \pi r_0^2 A^{2/3}$, with corrections ($r_0 \sim 1$ fm). To interpolate the experimental data for the total, inelastic, and elastic cross sections, the following expression is used:

$$\sigma(T, A) = \pi\left[r_0 A^{1/3} + \lambda(T, A)\right]^2 f(T)\phi(A)^{\alpha(T)}\,, \tag{5}$$

where λ is the de Broglie wavelength of the incident hadron in the hadron–nucleus center-of-mass system, T is the hadron's kinetic energy in the laboratory frame, A is the atomic weight of the nucleus, and $r_0 \sim 1$ fm corresponds to the nucleon radius. The functions $f(T)$, $\phi(A)$ and $\alpha(T)$ are represented by series of the following type:

$$\sum_i a_i T^{b_i}\,, \quad \sum_i a_i A^{b_i}\,. \tag{6}$$

The main drawback of the optical model is the prediction of a constant cross section for very high energies (> 100 GeV). The introduction of a relativistic increase in the nucleon radius, $r_0(T)$, overestimates the increase in the integral hadron–nuclear cross sections. This is the main argument in favor of the practical use of the Glauber model to describe the hadron–nuclear cross sections in the energy range above 100 GeV.

2.2.2 Simplified Glauber–Gribov model. Within the framework of the simplified (Gaussian distribution of point-like nucleons in the nucleus) Glauber–Gribov model (with the introduction of a correction for screening due to inelastic interaction), integral cross sections are described by the following relations [18]:

$$\sigma_{tot}^{hA} = 2\pi R^2 \ln\left[1 + \frac{A\sigma_{tot}^{hN}}{2\pi R^2}\right], \quad \sigma_{in}^{hA} = \pi R^2 \ln\left[1 + \frac{A\sigma_{tot}^{hN}}{\pi R^2}\right], \tag{7}$$

$$\sigma_{prod}^{hA} = \pi R^2 \ln\left(1 + \frac{A\sigma_{in}^{hN}}{\pi R^2}\right), \quad \sigma_{el}^{hA} = \sigma_{tot}^{hA} - \sigma_{in}^{hA},$$
$$\sigma_{qe}^{hA} = \sigma_{in}^{hA} - \sigma_{prod}^{hA}, \tag{8}$$

$$\sigma_{sd}^{hA}(hA \to XA) = \pi R^2\left[\alpha - \ln(1+\alpha)\right],$$
$$\alpha = \frac{A\sigma_{tot}^{hN}}{2\pi R^2 + A\sigma_{tot}^{hN}}\,. \tag{9}$$

Here, σ_{tot}^{hA} and σ_{in}^{hA} are, respectively, the integral total and inelastic cross sections for the strong interaction of a hadron with a nucleus containing A nucleons. The reaction cross section is σ_{prod}^{hA}, and the cross sections σ_{el}^{hA} and σ_{qe}^{hA} correspond, respectively, to the elastic and quasi-elastic channels (nucleus breakup with nucleon ejection). The cross section σ_{sd}^{hA} can be approximately related to the single-particle (incident hadron) dissociation channel. The cross sections σ_{tot}^{hA} and σ_{in}^{hA} depend significantly on the total hadron–nucleon cross sections, σ_{tot}^{hN}, whereas the reaction cross section, the process with the formation of new hadrons, is naturally determined by the inelastic hadron–nucleon cross section, σ_{in}^{hN}. The radius R corresponds to the root-mean-square deviation of the spatial (Gaussian) distribution of the nucleons inside the nucleus and can be considered to some extent as a free parameter of the model. This parameter is close to the expression $r_0 A^{1/3}$, $r_0 \sim 0.9-1.1$ fm. The latter value differs from the value of the proton charge radius (~ 0.7 fm) recommended in [22]. The difference is likely due to the influence of the strong interaction on the value of r_0. However, for light nuclei, R can be taken equal to the experimentally measured radius of the charge distribution in the nucleus, which still awaits a theoretical explanation.

The main advantage of the GG-model, in addition to its convenient analytical representation of a nearly complete set of the integral cross sections, is its prediction of a weak relativistic increase of the cross sections at incident hadron energies above 100 GeV due to a corresponding, though logarithmically weakened, increase in the cross sections of σ_{tot}^{hN} and σ_{in}^{hN}. Currently, the optical model is used in the Geant4 package for nucleons and pions in the energy range 0.01–90 GeV, while the GG-model is applied at higher energies. For the remaining hadrons in the entire range above 10 MeV, the GG-model is used.

2.3 Software design

Parameterizations for integral hadron–nucleon cross sections are contained in the Geant4 C++ class G4HadronNucleonXsc. The GG-model is implemented in the classes

- G4ComponentGGHadronNucleusXsc,
- G4BGGNucleonInelasticXS,
- G4BGGNucleonElasticXS,
- G4BGGPionInelasticXS,
- G4BGGPionElasticXS,

where the first class implements the GG-model, the others are responsible for combining the optical and GG-models (BGG-model), with its free parameter R slightly (no more than 3%) adjusted so that the cross sections are equal at an incident hadron energy of 91 GeV. Several interface classes support the inclusion of the CHIPS-model. All these classes are located in the source/processes/hadronic/cross sections subsection of the Geant4 software package.

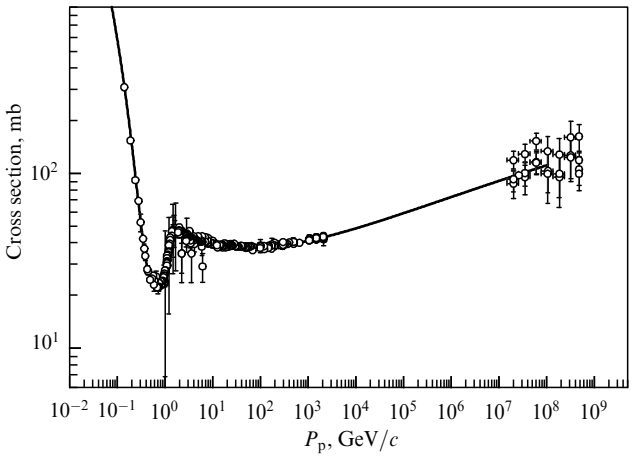

Figure 1. Integral total proton–proton cross section versus the proton momentum in the laboratory reference frame. The curve — Geant4 parametrization, the points — compilation of experimental data [8].

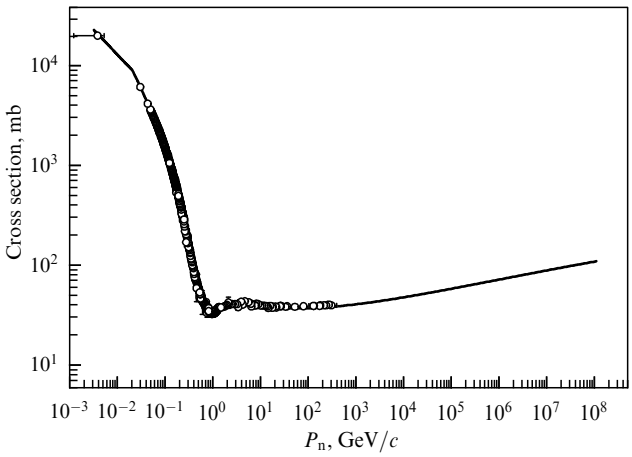

Figure 2. Integral total neutron–proton cross section versus the neutron momentum in the laboratory reference frame. The curve — Geant4 parametrization, the points — compilation of experimental data [8].

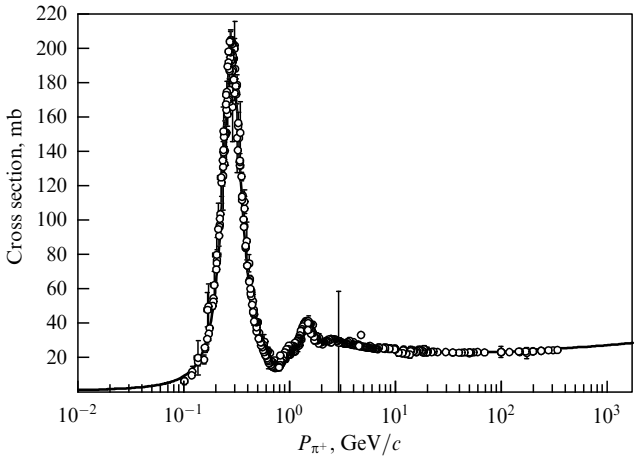

Figure 3. Integral total π^+-proton cross section versus the π^+ momentum in the laboratory reference frame. The curve — Geant4 parametrization, the points — compilation of experimental data [8].

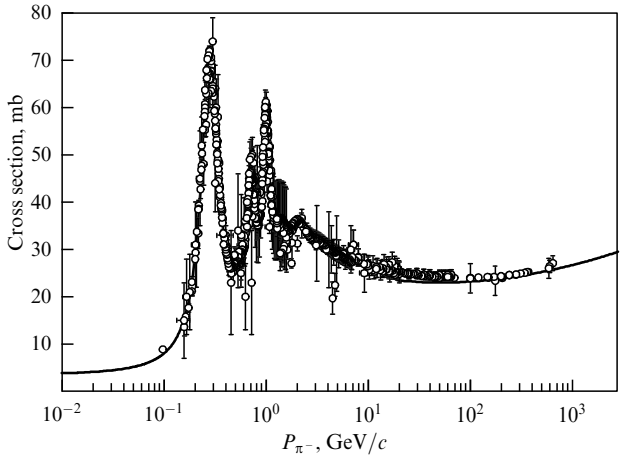

Figure 4. Integral total π^--proton cross section versus the π^- momentum in the laboratory reference frame. The curve — Geant4 parametrization, the points — compilation of experimental data [8].

3. Validation versus experimental data

3.1 Hadron–nucleon cross sections

Figures 1–4 show the integral total nucleon–nucleon and pion–nucleon cross sections as functions of the incident hadron momentum. The curves represent the Geant4 parameterizations, and the points represent a compilation of experimental data [8]. For positive hadrons that interact with protons at low energies, $T < 1$ MeV, the cross sections are corrected for the repulsive Coulomb barrier [23], which reflects the increasing contribution of the Coulomb electromagnetic interaction at low energies.

Figures 5–7 show the integral kaon-nucleon cross sections as functions of the kaon momentum. The curves represent the Geant4 parameterizations, and the points represent a compilation of experimental data [8]. Figure 8 shows the integral total cross sections of the Λ-particle and the Σ^--hyperon on a proton as functions of the hadron momentum (Λ, Σ^-). The curve corresponds to the integral total proton–proton cross section multiplied by the correction factor of 0.88 (it is this value, reflecting the significant similarity of the nucleon and hyperon cross sections, that presumably determines the relative contribution of the s-quark). The experimental points are a compilation of experimental data [8] for

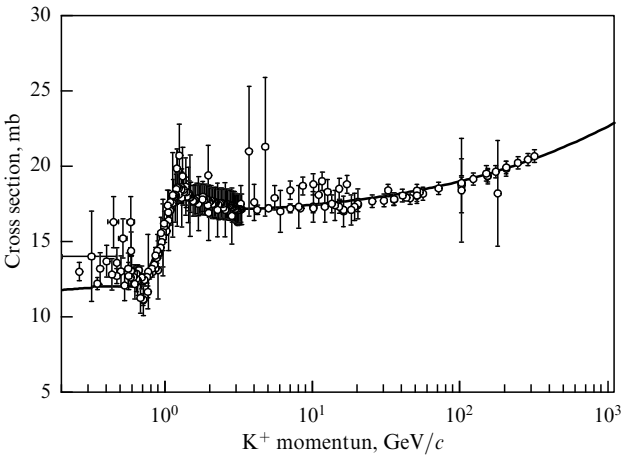

Figure 5. Integral total K^+-proton cross section versus the K^+ momentum in the laboratory reference frame. The curve — Geant4 parametrization, the points — compilation of experimental data [8].

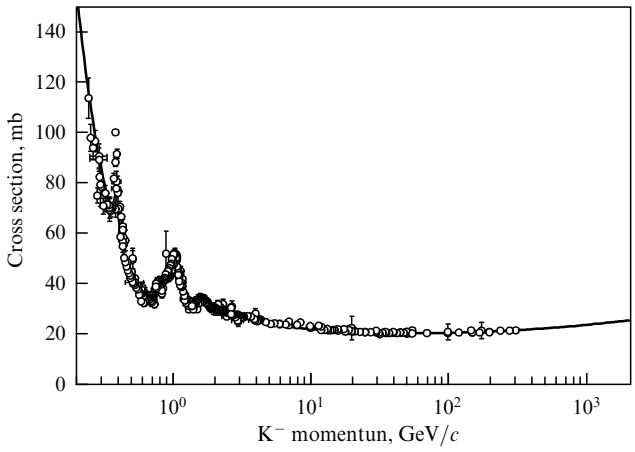

Figure 6. Integral total K^--proton cross section versus the K^- momentum in the laboratory reference frame. The curve — Geant4 parametrization, the points — compilation of experimental data [8].

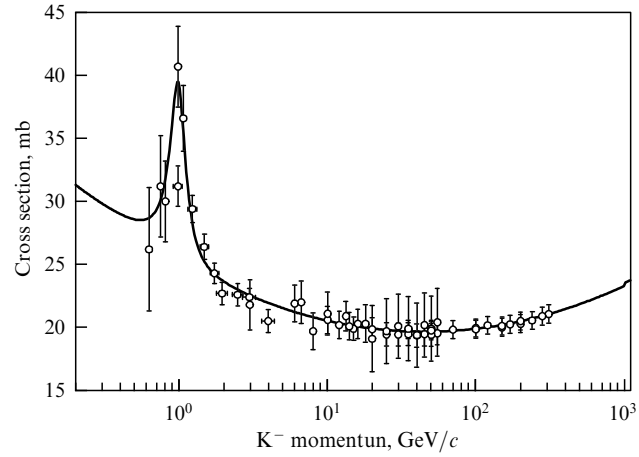

Figure 7. Integral total K^--neutron cross section versus the K^- momentum in the laboratory reference frame. The curve — Geant4 parametrization, the points — compilation of experimental data [8].

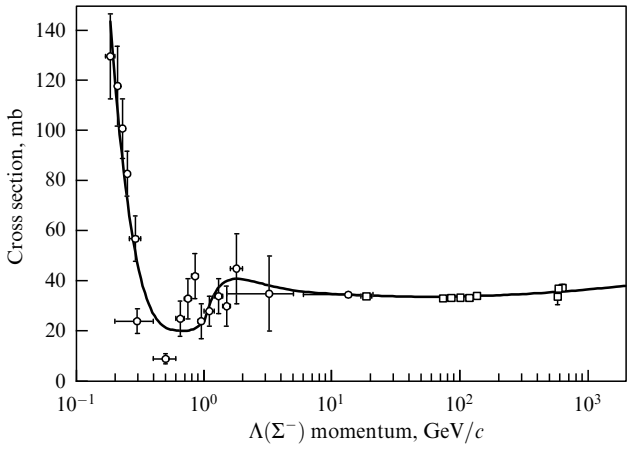

Figure 8. Combined $\Lambda(\Sigma^-)$–p cross section versus the $\Lambda(\Sigma^-)$ momentum in the laboratory reference frame. The curve — Geant4 parametrization for total proton–proton cross section multiplied by 0.88, the points — compilation of experimental data [8]: open circles — Λ–p, open squares — Σ^-–p.

the Λ-particle (open circles) and the Σ^--hyperon (open squares). Figure 9 shows the integral total cross sections of

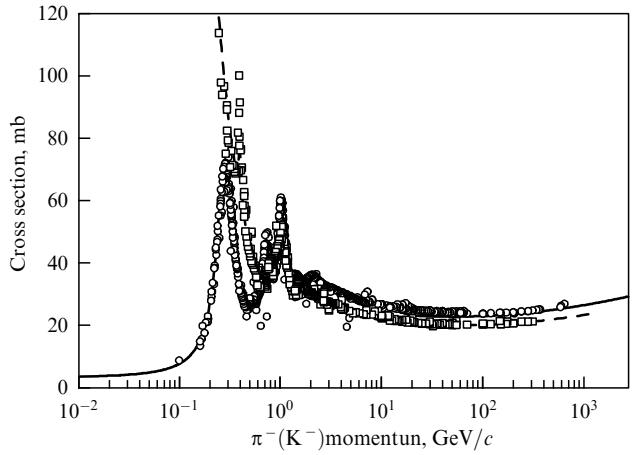

Figure 9. Integral total $\pi^-(K^-)$–p cross sections versus the meson momentum in the laboratory reference frame. The curves correspond to the Geant4 package parametrization: solid — π^-–p, dashed — K^-–p. The points — compilation of experimental data [8]: open circles — π^-–p, open squares — K^-–p.

negative pions and kaons on a proton versus the meson momentum. The curves are Geant4 parameterizations, the points are experimental data compilations [8]. The cross section ratio at energies greater than 5 GeV is 0.82 according to the quark additivity approach, $(\tilde{s} + 1/3)/(2/3) \simeq 0.82$.

3.2 Hadron–nuclei cross section

Figures 10–12 show the integral inelastic cross sections of the proton on the nuclei of carbon, aluminum and lead versus the kinetic energy of the proton, respectively. The curves represent the BGG-model, and the points represent a compilation of experimental data [9, 24]. Note that Fig. 10 shows the B-model (solid line) and the GG-model separately for the inelastic cross section (dashed line) and the reaction cross section (dotted line). It is evident that the B-model predicts a constant cross section at proton energies above 100 GeV, while the GG-model shows a weak relativistic increase in this region, consistent with the experimental data. Several experimental points (open squares) correspond more closely to the reaction cross section, as evidenced by the dotted line passing through them.

Similar curves for neutron interactions (total cross sections) with helium, carbon, and lead nuclei are shown in Figs 13–15. Figure 14 also shows the inelastic cross section (dashed line) and the reaction cross section (dotted line) according to the GG-model. The points correspond to experimental data: the total cross section is indicated by solid circles, and the inelastic cross section is indicated by open circles. The GG-model is in satisfactory agreement for the total and inelastic cross sections. Some experimental points for the inelastic cross sections can likely be attributed to the reaction cross section, since the dotted line passes through them. Below approximately 500 MeV, the GG-model provides a poorer fit to the experimental data, so the B-model is used for nucleons and pions.

Figure 16 shows the integral total cross section of a positive pion on an aluminum nucleus as a function of the kinetic energy of the pion. The curves represent the BGG-model, and the points represent a compilation of experimental data [9]. Similar curves for the interaction of negative pions with a carbon nucleus are shown in Fig. 17, 18 for the total and inelastic cross sections, respectively.

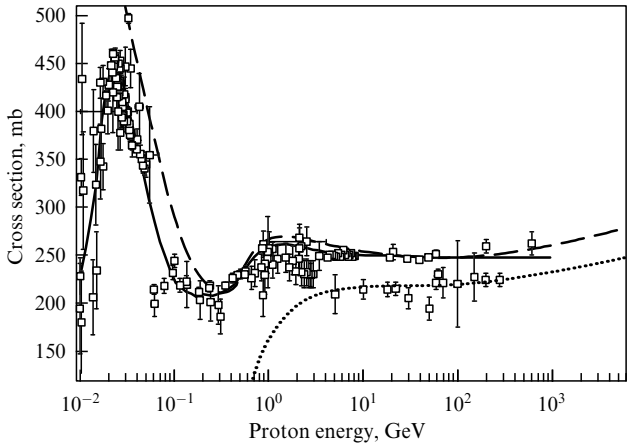

Figure 10. Integral inelastic cross section of proton scattering on carbon nuclei versus the kinetic energy of the proton in the laboratory reference frame. The curves: solid — B-model, dashed — GG-model, dotted — GG-model for reaction cross section. The points — compilation of experimental data [9, 24].

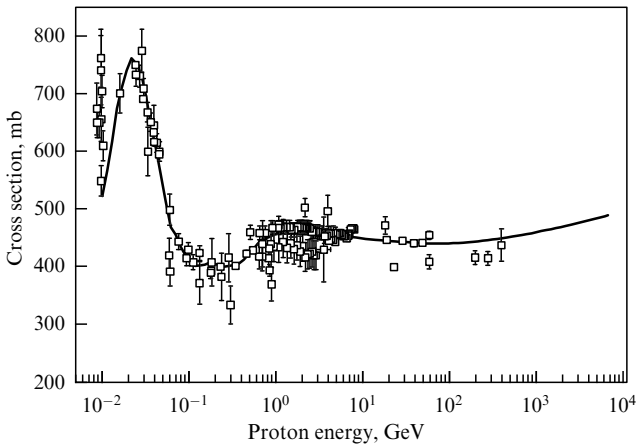

Figure 11. Integral inelastic cross section of proton scattering on aluminum nuclei versus the kinetic energy of the proton in the laboratory reference frame. The curve — BGG-model, the points — compilation of experimental data [9, 24].

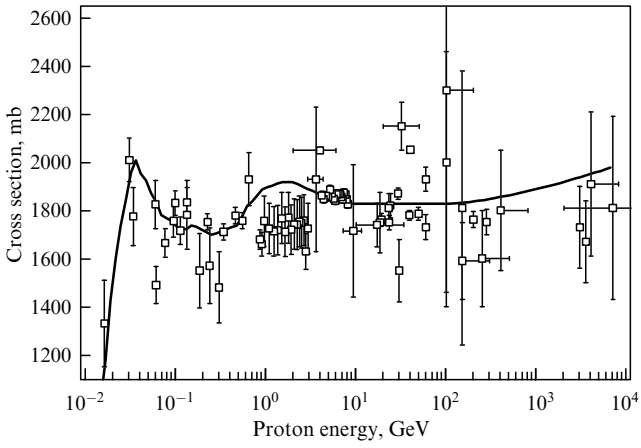

Figure 12. Integral inelastic cross section of proton scattering on lead nuclei versus the kinetic energy of the proton in the laboratory reference frame. The curve — BGG-model, the points — compilation of experimental data [9, 24].

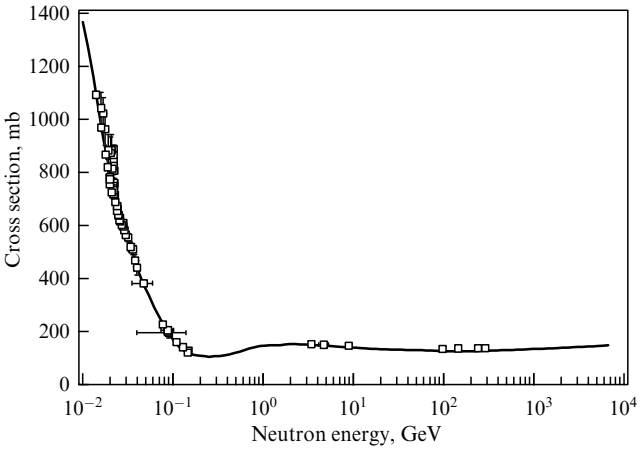

Figure 13. Integral inelastic cross section of neutron scattering on helium nuclei versus the kinetic energy of the neutron in the laboratory reference frame. The curve — BGG-model, the points — compilation of experimental data [9, 24].

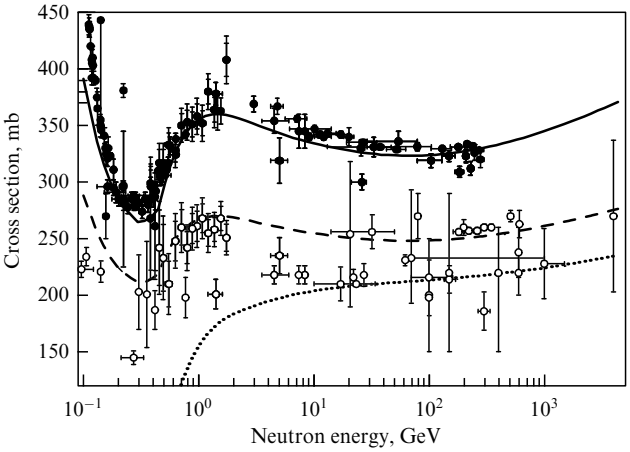

Figure 14. Integral total, inelastic cross sections and reaction cross section of neutron on carbon nuclei versus the kinetic energy of the neutron in the laboratory reference frame. The curves correspond BGG-model: solid — total cross section, dashed — inelastic and dotted — reaction cross section. The points — compilation of experimental data [9, 24].

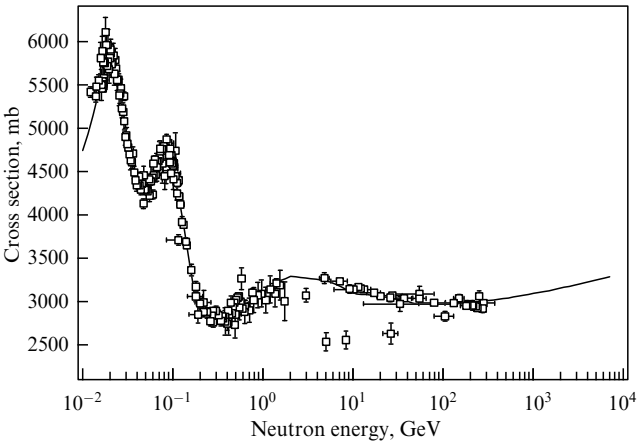

Figure 15. Integral total cross section of neutron scattering on lead nuclei versus the kinetic energy of the neutron in the laboratory reference frame. The curve — BGG-model, the points — compilation of experimental data [9, 24].

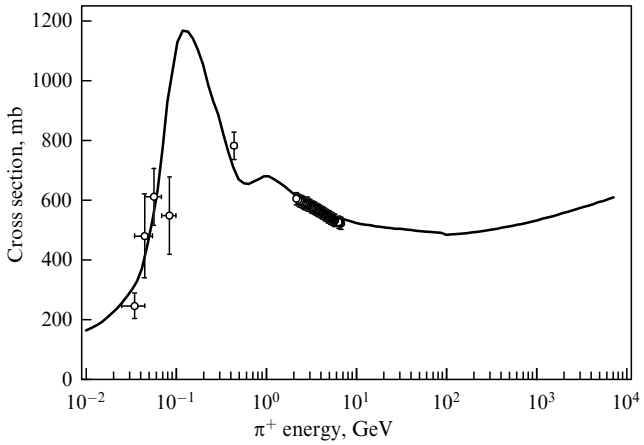

Figure 16. Integral total cross section of π^+ scattering on aluminum nuclei versus the kinetic energy of π^+ in the laboratory reference frame. The curve — BGG-model, the points — compilation of experimental data [9].

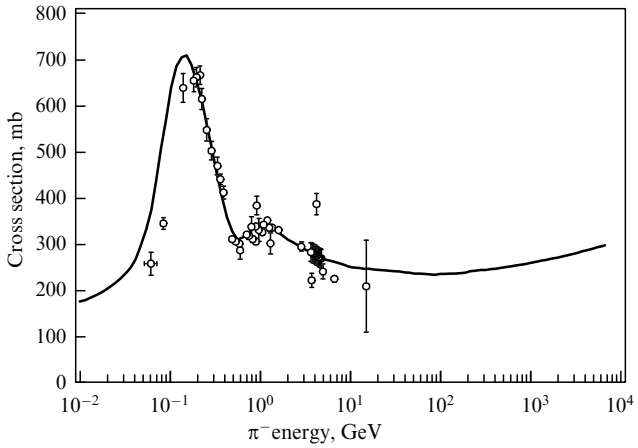

Figure 17. Integral total cross section of π^- scattering on carbon nuclei versus the kinetic energy of π^- in the laboratory reference frame. The curve — BGG-model, the points — compilation of experimental data [9].

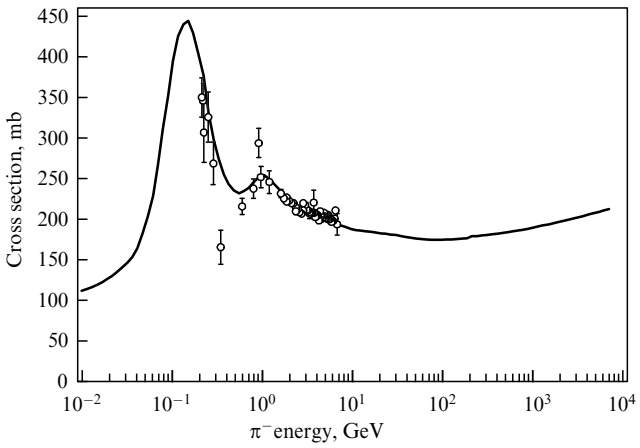

Figure 18. Integral inelastic cross section π^- scattering on carbon nuclei versus the kinetic energy of π^- in the laboratory reference frame. The curve — BGG-model, the points — compilation of experimental data [9].

Figures 19, 20 show the integral total cross section of positive kaons on the carbon and silicon nuclei, respectively, as

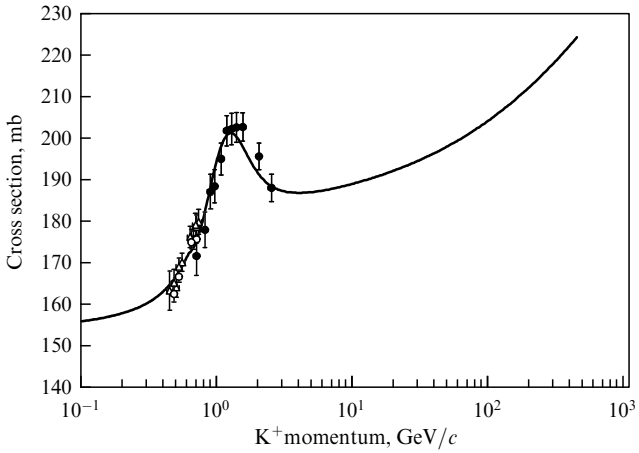

Figure 19. Integral inelastic cross section K^+ scattering on carbon nuclei versus the kinetic energy of K^+ in the laboratory reference frame. The curve — GG-model, the points correspond to experimental data: open circles [29], triangles [30] and solid circles [31].

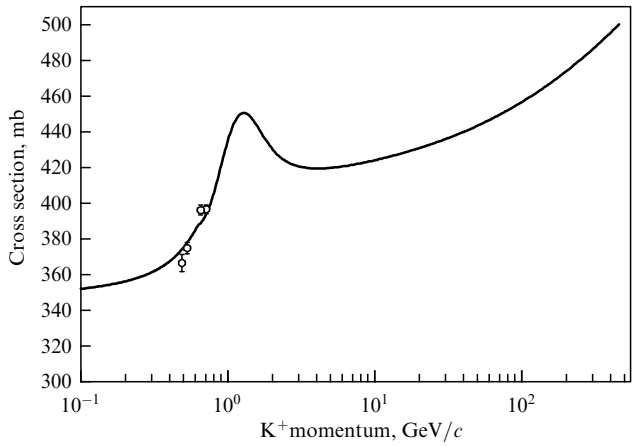

Figure 20. Integral inelastic cross section K^+ scattering on silicon nuclei versus the kinetic energy of K^+ in the laboratory reference frame. The curve — GG-model, the points correspond to experimental data [30].

a function of the kaon kinetic energy. The curves represent the GG-model. For carbon, the experimental data correspond to open circles [29], triangles [30], and solid circles [31]. For silicon, the points correspond to experimental data [30].

For the interaction of positive hadrons with nuclei at low energies, a correction was introduced for the repulsive Coulomb barrier [23].

4. Discussion

Calculated and experimental cross sections can be compared using statistical methods, such as the Pearson χ^2 test [32, 33]. The value of χ^2 is estimated as:

$$\chi^2 = \sum_{i=1}^{n} \frac{\left(\sigma(T_i) - \sigma_i\right)^2}{\delta\sigma_i^2}\,, \tag{10}$$

where σ_i, $\delta\sigma_i$ and T_i are the cross section, its standard deviation, and the kinetic energy, respectively, from a file of experimental values with n points. The calculated cross section at energy T_i is denoted as $\sigma(T_i)$. A qualitative assessment of the calculation and experiment can be

achieved using the reduced value of $\langle\chi^2\rangle$:

$$\langle\chi^2\rangle = \frac{\chi^2}{n} \leqslant 1\,. \tag{11}$$

Asymptotically, for $n \to \infty$, the value of χ^2 is distributed according to the Γ-function, which opens the possibility of numerically assessing the agreement between the calculation and experiment. The χ^2 criterion can be compared with other empirical methods (the bottom two rows of the Table 3 for the inelastic proton–carbon interaction) to estimate the mean deviations of [34]:

$$\left\langle \frac{|\Delta|}{\delta} \right\rangle = \frac{1}{n}\sum_{i=1}^{n} \frac{|\sigma(E_i) - \sigma_i|}{\delta\sigma_i}\,,$$
$$\left\langle \left| \ln \frac{\sigma^{\mathrm{mod}}}{\sigma^{\mathrm{exp}}} \right| \right\rangle = \frac{1}{n}\sum_{i=1}^{n} \left| \ln \frac{\sigma(E_i)}{\sigma_i} \right|. \tag{12}$$

However, the distributions of these quantities are not described by standard special functions [34].

Tables 3–7 show the values of $\langle\chi^2\rangle$ for protons, neutrons, and pions in nuclei, respectively. It is clear that the BGG-model provides, on average, lower values of $\langle\chi^2\rangle$ for those nuclei for which experimental data are available. This is the main reason why the BGG- and GG-models are used in most of the physical lists of the Geant4 software package over a wide range of incident hadron energies, including heavy baryons and mesons, and for nuclei from hydrogen to uranium inclusive, despite the fact that they are not free of empirical parameters.[1] Note that the experimental data for integral inelastic cross sections have a much more pronounced scatter than the data for total cross sections. This is because it is not always possible to identify with sufficient accuracy the production of new hadrons, i.e., the process corresponding to the reaction cross section. However, since the inelastic cross section includes both the reaction cross section and the quasi-elastic process, this difference is not fundamental in most cases.

[1] At the All-Moscow Seminar on Theoretical Physics, which he chaired, V.L. Ginzburg repeatedly emphasized — "The proof of the pudding is in the eating."

Table 3. $\langle\chi^2\rangle$ values for various inelastic p–A integral cross sections.

Inelastic p–A cross sections	$\langle\chi^2\rangle$, BGG	$\langle\chi^2\rangle$, AHPW	$\langle\chi^2\rangle$, LHEP	n
p–Al	0.318	1.50	1.07	136
p–Si	0.105	0.515	0.551	61
p–Si (< 1 GeV)	0.029	0.683	0.502	44
p–Fe	0.519	6.46	0.86	64
p–Cu	0.51	16.9	0.604	82
p–Pb	0.479	11	1.56	87
p–U	0.182	0.847	0.176	52
p–C	0.468	2.45	0.738	172
p–C, $\langle\lvert\Delta\rvert/\delta\rangle$	0.437	0.97	0.639	172
p–C, $\langle\lvert \ln(\sigma^{\mathrm{mod}}/\sigma^{\mathrm{exp}})\rvert\rangle$	0.066	0.132	0.096	172

Table 4. $\langle\chi^2\rangle$ values for various n–A cross sections.

n–A cross sections	$\langle\chi^2\rangle$, BGG	$\langle\chi^2\rangle$, AHPW	$\langle\chi^2\rangle$, LHEP	n
n–C inelastic	0.413	0.469	0.793	73
n–Fe inelastic	0.624	0.539	1.08	39
n–Cu inelastic	0.395	0.720	0.491	49
n–W inelastic	0.07	0.109	0.173	9
n–Pb inelastic	0.130	0.157	0.255	53
n–U inelastic	0.190	0.395	0.500	33
n–He total	1.44	—	17.37	65
n–C total	0.767	—	9.89	309
n–Fe total	0.514	—	1.89	120
n–Cu total	0.487	—	1.97	206
n–W total	0.257	—	1.26	24
n–Pb total	0.587	—	3.76	209

Table 5. $\langle\chi^2\rangle$ values for total π–A cross sections.

Model/total $\pi^{\pm}$–A cross sections	$\langle\chi^2\rangle$, LHEP	$\langle\chi^2\rangle$, CHIPS	$\langle\chi^2\rangle$, BGG
π^-–He	1.1	1.5	1.6
π^-–Be	0.89	0.98	0.21
π^-–C	0.35	0.25	0.16
π^-–O	0.31	0.4	0.02
π^-–F	0.34	0.34	0.36
π^-–Al	0.88	0.98	0.89
π^-–Cu	1.53	0.61	0.35
π^-–Au	0.24	0.34	0.19
π^+–C	0.36	0.25	0.17
π^+–Al	0.79	0.37	0.76

Table 6. $\langle\chi^2\rangle$ values for inelastic π–A cross sections.

Model/inelastic $\pi^+ - A$ cross sections	$\langle\chi^2\rangle$, LHEP	$\langle\chi^2\rangle$, CHIPS	$\langle\chi^2\rangle$, BGG
π^+–Be	0.44	0.98	0.34
π^+–C	0.11	0.39	0.13
π^+–Al	0.31	1.02	1.97

Thus, the precision of Geant4 corresponds to the accuracy of the experimental data and is at the level of a few percent. If this accuracy is insufficient for modeling specific processes, Geant4 allows the user to add a more accurate description for a specific pair of incident hadron–target nucleus. This can be done in the form of a cross section table or using analytical formulas. To study the influence of systematic cross section errors on the final results, a constant factor can be applied across the entire energy range, increasing or decreasing the cross section.

Table 7. $\langle\chi^2\rangle$ values for elastic π–A cross sections.

Model/elastic π^- – A cross sections	$\langle\chi^2\rangle$, LHEP	$\langle\chi^2\rangle$, CHIPS	$\langle\chi^2\rangle$, BGG
π^-–He	1.82	3.48	0.98
π^-–Be	2.9	4.0	1.5
π^-–C	2.23	2.24	0.80
π^-–N	1.2	2.6	0.3
π^-–O	1.3	2.4	0.08
π^-–Al	3.1	2.0	0.9
π^-–Au	1.6	1.6	1.0

5. Conclusions

This review presents the history of the development of approaches to describe hadron cross sections in Geant4, which has been ongoing for about 25 years. The need to provide modeling for a wide range of applications in various fields of science and engineering naturally support the approach described in this paper. A distinctive feature of Geant4 is its openness to new alternative solutions to problems, which is fully applicable to hadron cross sections. Therefore, it is possible to develop cross section models based on new accurate data and precise theoretical calculations.

It is interesting to note that the GG-model provides a satisfactory description of integral nucleus-nucleus cross sections over a wide range of energies and atomic weights. This observation will be discussed elsewhere.

The authors thank M.V. Kosov and N.I. Starkov for helpful advice on the parametrization structure of hadron–nucleon cross sections in the resonance region.

This research was supported by a grant from the Government of the Russian Federation (Agreement No. 075-15-2025-009 dated February 28, 2025).

References

1. Dremin I M *Sov. Phys. Usp.* **26** 993 (1983); *Usp. Fiz. Nauk* **141** 517 (1983)
2. Dremin I M *Sov. Phys. Usp.* **31** 462 (1988); *Usp. Fiz. Nauk* **155** 139 (1988)
3. Levin E M, Ryskin M G *Sov. Phys. Usp.* **32** 479 (1989); *Usp. Fiz. Nauk* **158** 177 (1989)
4. Bertini M, Giffon M *Phys. Part. Nucl.* **26** 12 (1995); *Fiz. Elem. Chast. Atom. Yad.* **26** 32 (1995)
5. Kopeliovich B Z *Phys. Rev. C* **68** 044906 (2003)
6. Glauber R J, in *High-Energy Physics and Nuclear Structure. Proc. of the Third Intern. Conf. on High Energy Physics and Nuclear Structure, Columbia Univ., New York City, September 8–12, 1969* (Ed. S Devons) (New York: Plenum Press, 1970) p. 207, DOI:10.1007/978-1-4684-1827-9_43; Translated into Russian: *Usp. Fiz. Nauk* **103** 641 (1971)
7. Gribov V N *Sov. Phys. JETP* **29** 483 (1969); *Zh. Eksp. Teor. Fiz.* **56** 892 (1969)
8. Tanabashi M et al. (Particle Data Group) *Phys. Rev. D* **98** 030001 (2018)
9. Barashenkov V S, Toneev V D *Vzaimodeistviya Vysokoenergeticheskikh Chastits i Atomnykh Yader s Yadrami* (Interactions of High-energy Particles and Atomic Nuclei with Nuclei) (Moscow: Atomizdat, 1972)
10. Agostinelli S et al. *Nucl. Instrum. Meth. Phys. Res. A* **506** 250 (2003)
11. Allison J et al. *IEEE Trans. Nucl. Sci.* **53** 270 (2006)
12. Allison J et al. *Nucl. Instrum. Meth. Phys. Res. A* **835** 186 (2016)
13. Ranft J *Part. Accel.* **3** 129 (1972)
14. Wellisch H P, Axen D *Phys. Rev. C* **54** 1329 (1996)
15. Barashenkov V S "Pion-yadernye secheniya" ("Pion-nucleus cross sections"), Communication of JINR P2-90-158 (Dubna: JINR, 1990)
16. Barashenkov V S "Nuklon-yadernye secheniya" ("Nucleon-nucleus cross sections"), Communication of JINR P2-89-770 (Dubna: JINR, 1989)
17. Degtyarenko P V, Kossov M V, Wellisch H-P *Eur. Phys. J. A* **8** 217 (2000)
18. Grichine V M *Eur. Phys. J. C* **62** 399 (2009)
19. Lipkin H J *Nucl. Phys. B* **78** 381 (1974)
20. Anisovich V V et al. *Sov. Phys. Usp.* **27** 901 (1984); *Usp. Fiz. Nauk* **144** 553 (1984)
21. Biagi S F et al. *Nucl. Phys. B* **186** 1 (1981)
22. Khabarova K Yu, Kolachevsky N N *Phys. Usp.* **64** 1038 (2021); *Usp. Fiz. Nauk* **191** 1095 (2021)
23. Guèye P et al. *Phys. Rev. C* **60** 044308 (1999)
24. Barashenkov Compilation of cross sections for nucleon induced reactions at energies above a few MeV (Prepared by S. Mashnik), https://www.oecd-nea.org/dbdata/bara.html
25. Plompen A J M et al. *Eur. Phys. J. A* **56** 181 (2020)
26. Zmeškal M et al. *Ann. Nucl. Energy* **211** 110914 (2025)
27. Bagulya A V, Grishin V M, Ivanchenko V N, Chalyi N A *Izv. Vyssh. Ucebn. Zaved. Fiz.* **67** (12) 80 (2024)
28. TENDL-2023, https://tendl.web.psi.ch/tendl_2023/tendl2023.html
29. Krauss R A et al. *Phys. Rev. C* **46** 655 (1992)
30. Friedman E et al. *Phys. Rev. C* **55** 1304 (1997)
31. Bugg D V et al. *Phys. Rev.* **168** 1466 (1968)
32. Hudson D J *Statistics* (Geneva: CERN, 1964)
33. Cowan G *Statistical Data Analysis* (Oxford: Clarendon Press, 1998)
34. Sheskin D J *Handbook of Parametric and Nonparametric Statistical Procedures* 2nd ed. (Boca Raton, FL: Chapman and Hall, CRC, 2000)